Near-Infrared Light-Driven Shape-Morphing of Programmable Anisotropic Hydrogels Enabled by MXene Nanosheets

Pan Xue, [a] Hari Krishna Bisoyi, [b] Yuanhao Chen,[a] Hao Zeng,[c] Jiajia Yang,[a] Xiao Yang,[a] Pengfei Lv, [a] Xinmu Zhang,[a] Arri Priimagi,[c] Ling Wang,*[a] Xinhua Xu,*[a] and Quan Li*[b]

[a] School of Materials Science and Engineering, Tianjin University, Tianjin 300350, China. *E-mail: lwang17@tju.edu.cn (L.W.); xhxu@tju.edu.cn (X.X.)
[b] Advanced Materials and Liquid Crystal Institute and Chemical Physics Interdisciplinary Program, Kent State University, Kent, Ohio 44242, USA. *E-mail: quanli3273@gmail.com (Q.L.)
[c] Smart Photonic Materials, Faculty of Engineering and Natural Sciences, Tampere University, P.O. Box 541, Tampere, FI-33101 Finland

Abstract: Synthetic materials, that are soft, photoresponsive, programmable and capable of versatile shape-morphing, have become an emerging paradigm for the development of next-generation smart robots with wireless controllability and biomimetic functions. Herein, we report near-infrared (NIR) light-driven shape-morphing of programmable MXene-containing anisotropic hydrogel actuators that are fabricated through *in situ* free-radical copolymerization of a judiciously designed MXene nanomonomer with thermosensitive hydrogel network. A low electric field (few V mm^{-1}) was found to enable a spatial distribution of MXene nanosheets and hence introduce the anisotropy into the hydrogel network. Programmable anisotropic hydrogel actuators were developed by controlling ITO electrode pattern, direct-current (DC) electric field direction and mask-assisted photopolymerization. As a proof-of-concept, we demonstrated NIR light-driven shape morphing of the MXene-containing anisotropic hydrogel into various shapes and devise a four-arm soft gripper that can perform distinct photomechanical functions such as grasping, lifting/lowering down and releasing an object upon sequential NIR light exposure. The proposed strategy would provide impetus into the development of programmable and reconfigurable smart actuators that can find promising applications in diverse areas such as soft robotics or machines, biomedical devices and beyond.

Introduction

Smart actuators that can generate active force and controlled motions in response to applied stimuli are ubiquitous in nature and biological systems with well-defined hierarchical nanostructures.[1] For instance, human body movements are driven by the directional contraction of skeletal muscles with longitudinally aligned cylindrically-shaped muscle fibers.[2] The adaptive motions of many plants such as opening/closing of pinecones upon exposure to humidity changes, in turn, are dictated by the water dehydration/absorption of the tissues with anisotropically oriented cellulose fibrils.[3] The built-in anisotropy in biological systems plays a key role in promoting efficient force generation, precise movement and possibility of mass transport between/within species, which together form the basis for versatile natural adaptation. Taking inspiration from nature, extensive efforts have been devoted to the development of artificial smart actuators based on responsive soft materials, such as liquid crystal polymer networks, shape memory polymers, and polymeric hydrogels.[4] Among them, hydrogels are known to exhibit large shape-changes when subjected to heat/light stimulus, and possess significant advantages such as tissue-like softness and superior biocompatibility, thus receiving tremendous attention in soft robotics, drug delivery and tissue scaffold engineering.[5]

In general, shape morphing of hydrogel actuators is attributed to the volume change (by swelling/deswelling) associated with the uptake/release of water within the crosslinked polymer networks. Such volume responsiveness can be attained by exposure to various stimuli, such as humidity, temperature, light, pH, and magnetic/electric fields.[4]f,[6] Among them, light is particularly attractive for the realization of untethered soft robots, due to its ubiquity and controllability with high spatial and temporal accuracy; and remote NIR light is often much preferred over the UV or the visible in areas of biomedical and materials science thanks to its invisibility and superior tissue penetration depth.[7] Conventional photoresponsive hydrogels are usually fabricated by direct polymerization of molecular components homogeneously dissolved in aqueous media, thus exhibiting chemical/structural homogeneity and ineligible for anisotropic deformation or programmable actuation.[8] The attempts to obtain shape-programmable smart hydrogels involve building up three-dimensional (3D) material architectures with anisotropic mechanical property, and integration of aligned nanomaterials or patterning of functional nanoparticles within the hydrogel network.[9] However, these efforts require sophisticated fabrication techniques such as 3D printing, or challenging chemical synthetic procedures. It is highly desirable to develop facile fabrication approaches to obtain programmable anisotropy in hydrogels for on-demand spatiotemporal actuation.

Recently, the integration of two-dimensional (2D) nanomaterials with hydrogel frameworks has become an emerging technique for realizing shape-programmable soft actuators. The incorporated 2D nanomaterials not only enhance the mechanical properties of polymeric hydrogels, but also endow hydrogel actuators with new functionalities. For instance, Aida *et al.* reported a thermoresponsive hydrogel capable of large and programmable deformation by integrating co-facially oriented uni-lamellar electrolyte titanate nanosheets (TiNSs) into poly(N-isopropylacrylamide) (PNIPAM) hydrogels.[10] Wu *et al.* developed robust hydrogels with spatially ordered structures by using multiple electrodes to program the distribution of electric field that could induce spatial orientations of highly charged fluorohectorite nanosheets before the polymerization and crosslinking of PNIPAM hydrogels.[11] In other examples, hexagonal boron nitride facilitates thermal actuation with fast response speed,[12] and reduced graphene oxide enables fast inverse snapping motion in an anisotropic hydrogel.[13] Among multitudinous 2D nanomaterials, $Ti_3C_2T_x$ MXenes, discovered by Yury Gogotsi's lab in 2011, have received rapidly increasing attention, thanks to their unprecedented combination of multiple promising characteristics such as excellent hydrophilicity, outstanding thermal/electrical conductivity and high photothermal conversion efficiency.[14] Several MXene-based smart actuators responding to electrochemical signals,[15] environmental humidity,[16] and leaf-inspired multiresponsive MXene actuators have recently been reported.[17] However, shape-programmable smart actuators based on MXene-loaded hydrogels remain scarce.[18] It is anticipated that the "marriage" between anisotropic MXene

nanosheets and isotropic hydrogels would potentially yield soft actuators with programmable photomechanical functionalities.

Herein, we report a NIR light-driven MXene-containing anisotropic hydrogel actuator with shape programmability, which was fabricated through *in situ* free-radical copolymerization of a judiciously designed photopolymerizable MXene nanomonomer with thermosensitive PNIPAM hydrogels (**Figure 1**). A low electric field (few V mm^{-1}) was used to induce concentration gradient of MXene nanosheets across the thickness of the hydrogel, yielding tailorable network density and structural anisotropy. ITO-patterned electric fields and mask-assisted photopolymerization were applied for developing shape-programmable MXene-containing anisotropic hydrogel actuators, which could exhibit shape-transformation into various geometries, such as “U”, “J”, “S”, “Ω” and complex “flower” shapes upon NIR light exposures. As a proof-of-concept robotic functionality, we demonstrated a four-arm soft gripper performing distinct photomechanical functions including grasping, lifting up, lowering down, and releasing an object under sequential NIR light irradiation. We believe that these MXene-containing anisotropic hydrogel actuators with programmable photomechanical functions could shine new light into the development of untethered, adaptive and reconfigurable biomimetic soft robotics.

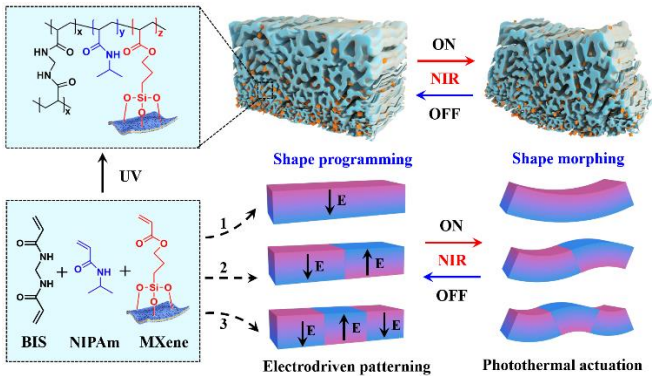

Figure 1. Materials, structure, electrodriven shape-programming and NIR light-driven shape-morphing of MXene-containing anisotropic hydrogel actuators.

Results and Discussion

To promote homogeneous dispersity of MXene nanosheets and *in situ* photopolymerization into 3D crosslinked hydrogel networks, we designed and synthesized a surface functionalized photopolymerizable MXene nanomonomer, through uniformly coating thin mesoporous-silica layer onto the surface of exfoliated ultrathin MXene, followed by covalent conjugation of photopolymerizable 3-(trimethoxysilyl)propyl methacrylate (TMSPMA), as shown schematically in **Figure 2a**. To be more specific: (1) ultrathin MXene were firstly synthesized by exfoliating the bulk layer-structured Ti_3AlC_2 MAX-phase via initial hydrofluoric acid (HF) etching with subsequent intercalation of tetrapropylammonium hydroxide (TPAOH); (2) The negatively charged surface of ultrathin MXene was then coupled with positively charged cetyltrimethylammonium chloride (CTAC) via electrostatic interaction, and MXene@$mSiO_2$ was developed by the *in situ* growth of a mesoporous-silica layer onto the surface of CTAC-adsorbed MXene with tetraethylorthosilicate (TEOS) as silica source under alkaline condition; (3) MXene nanomonomer was subsequently achieved by grafting TMSPMA onto the surface of MXene@$mSiO_2$ via silanization. Further details about the synthetic process are given in the Supporting Information (**Figure S1-S6**).

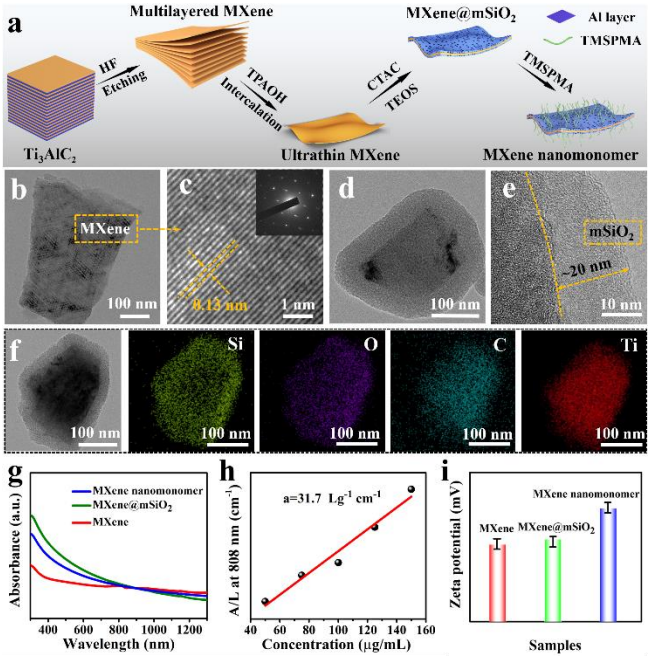

Figure 2. Synthesis and characterizations of photopolymerizable MXene nanomonomer. (a) Schematic process of synthesizing MXene nanomonomer. (b) TEM image of the ultrathin MXene. (c) Magnified TEM image of the ultrathin MXene, where the inset shows the corresponding SAED pattern. (d) Low and (e) high resolution TEM images of the MXene nanomonomer. (f) The elemental-mapping images of MXene nanomonomer (Si, O, C, and Ti elements). (g) UV-Vis spectra of MXene, MXene@SiO_2 and MXene nanomonomer dispersions in deionized water. (h) Normalized absorbance intensity at λ = 808 nm divided by the characteristic length of the cell (A/L) at varied concentrations (50, 75, 100, 125, and 150 μg mL^{-1}). (i) The zeta potentials of MXene, MXene@SiO_2 and MXene nanomonomer dispersions in deionized water.

High-resolution transmission electron microscopy (HRTEM) was implemented to characterize the nanostructures of ultrathin MXene and as-prepared MXene nanomonomer. The high-resolution images (**Figure 2b, c**) show that the constant interplanar distance is ~ 0.13 nm and MXene exhibits a hexagonal crystalline nature, as shown by the selected area electron diffraction (SAED) pattern in the inset of **Figure 2c**. A uniform mesoporous-silica layer is clearly visible on the surface of MXene nanomonomer as evidenced by TEM images and elemental-mapping of energy dispersive X-ray spectrometry (EDS) (**Figure 2d-f**). X-ray photoelectron spectroscopy (XPS) also indicates the characteristic peaks of MXene nanomonomer at 455.2, 459.5, and 103.4 eV, which can be indexed as Ti-C, Ti-O, and Si-O bonds, respectively (**Figure S7**).[19] Moreover, N_2 adsorption desorption isotherm and corresponding pore-size distribution indicate a successful formation of mesoporous structure on the surface of MXene nanomonomer with large surface area of ~ 690 m^2 g^{-1}, and attaining uniformity of pore size of ~ 3.9 nm (**Figure S8**).

The dynamic light scattering characterization shows that the average hydrodynamic diameter of the MXene nanomonomer in deionized water is ~ 300 nm (**Figure S9**), and the surface coating of mesoporous SiO_2 led to a slight increase in the size of MXene nanomonomer. The MXene nanomonomer exhibited a high optical absorption across visible and near infrared range (400-900 nm) (**Figure 2g**). The extinction coefficient at 808 nm was measured to be ~ 31.7 Lg^{-1} cm^{-1} (**Figure 2h**, and **Figure S10**, see measurement in Supporting Information). This value is higher

than that of Ti_3C_2 nanosheets (~ 25.2 Lg^{-1} cm^{-1}), suggesting that the mesoporous-silica coating can enhance the photothermal capacity of $Ti_3C_2T_x$ MXene.[19][20] Compared with ultrathin MXene and MXene@$mSiO_2$, MXene nanomonomer exhibits a higher zeta potential (**Figure 2i**), which would be beneficial to the electrophoresis and migration of MXene nanosheets under applied DC electric field. Such electrophoretic mobility in solution under electric field is the key to program the actuation behavior of NIR light-driven MXene-containing anisotropic hydrogel actuators. In this work, 808 nm NIR light is applied for spatiotemporal actuation in an aqueous environment thanks to its much lower absorption by water (typical absorption coefficient is 0.02 cm^{-1} at 808 nm, in contrast to 0.48 cm^{-1} at 980 nm).[21] It should also be noted that the choice of irradiation wavelength is by no means limited and other wavelengths can be used if desired.

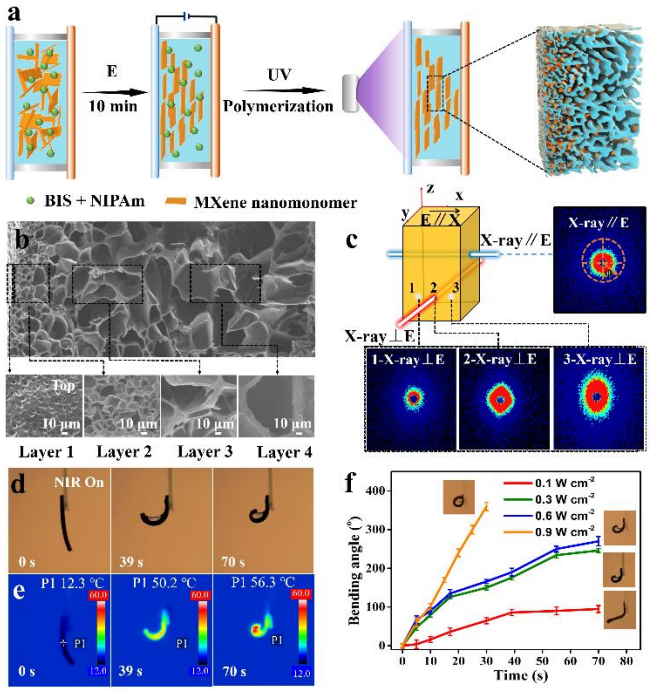

Figure 3. MXene-containing anisotropic hydrogels ($MX_{10}N_1$-E_2). (a) Schematic process of fabricating MXene-containing gradient hydrogels. (b) SEM images showing a cross-section view of the MXene-containing gradient hydrogel and SEM investigations on the surface morphology of different area, which indicates an increasing pore size from anode (left) to cathode (right) surface of the hydrogel. (c) 2D SAXS images of MXene-containing gradient hydrogel measured from parallel directions to the applied electric field (X-ray//E); and the ones measured from orthogonal direction to the applied electric field,1-X-ray⊥E, 2-X-ray⊥E and 3-X-ray⊥E correspond to different positions taken from the cathode (left) to the anode side (right), respectively. (d) Real images of MXene-containing hydrogel actuators ($MX_{10}N_1$-E_2) upon exposure to 808 nm NIR light (0.3 W cm^{-2}), and (e) the corresponding thermal imaging photographs of MXene-containing hydrogel actuators ($MX_{10}N_1$-E_2) upon exposure to 808 nm NIR light (0.3 W cm^{-2}). (f) Actuation performances of MXene-containing hydrogel actuators ($MX_{10}N_1$-E_2) upon being irradiated by 808 nm NIR light with different powers (0.1, 0.3, 0.6, and 0.9 W cm^{-2}).

To endow MXene-containing soft hydrogels with on-demand spatial anisotropy, a DC electric field was used to induce electrophoresis rendering concentration gradient of MXene nanomonomer within the reaction solution (**Figure 3a**). When the electric field is turned on, the MXene nanomonomer migrates toward the anode due to their negatively charged nature. The electric field was removed, and a photopolymerization (UV, 365 nm, 20 mW cm^{-2}, 10 min) was then carried out in an ice bath to obtain crosslinked hydrogel network, where the formation of covalent bonding between the polymer network and MXene nanomonomer was confirmed by Fourier-transform infrared spectroscopy (**Figure S11**). To characterize the structure in details, we note the hydrogel sample as MX_aN_1-E_b, where *a* and *b* represent the mass concentration of MXene nanomonomer (mg mL^{-1}) and the voltage of DC electric field (V mm^{-1}), respectively; and N_1 represents 400 mg of N-isopropylacrylamide (NIPAM) monomer, 20 mg of N,N'-methylenebis(acrylamide) (BIS), 5 μL of photoinitiator Darocur 1173 in 1 mL dimethyl sulfoxide (DMSO). **Figure 3b** shows the scanning electron microscopy (SEM) images of freeze-dried $MX_{10}N_1$-E_2 hydrogel sample, which exhibits a morphologic network gradient by forming different pore sizes across the thickness. Pores of the hydrogel network have a relatively large size (≈ 150 μm) near the cathode, and gradually decrease to about 10 μm at the region close to the anode. Interestingly, the $MX_{10}N_1$-E_2 hydrogels fabricated by photopolymerizing from the cathode side were found to exhibit similar microstructure characteristics as those photopolymerized from the anode side. Without the application of DC electric field, the hydrogel ($MX_{10}N_1$-E_0) with same chemical composition showed a relatively uniform network structure across the thickness of hydrogels (**Figure S12**). These results suggest that the formation of network gradient results from the MXene density distribution controlled by the electric field, not the UV light penetration depth during the polymerization process. EDX spectra also indicates that negatively charged MXene nanomonomer is inclined to move towards the anode under the DC electric field (**Figure S13**), which forms higher crosslinking density and denser hydrogel network during the photopolymerization process.

The anisotropy of MXene-containing hydrogel ($MX_{10}N_1$-E_2) was further confirmed by 2D small-angle X-ray scattering (SAXS) analysis. As shown in **Figure 3c**, elliptical diffusive patterns were observed in the direction orthogonal to the electric field, and an isotropic one in the parallel direction. Note that elliptical diffusive pattern is position dependent, indicating different orientation order of MXene along the sample thickness. Accordingly, the azimuthal angle (φ) plot of the 2D SAXS pattern measured from the orthogonal direction to the electric field has two peaks, at $\theta = 180°$ and 360°, whereas the measurement parallel to the electric field shows a single plateau (**Figure S14**). On the basis of the fitting of the azimuthal angle plots, the orientation degree of MXene nanomonomer can be calculated using the following equation:[6]d,e,[9]c

$$\Pi = (180° - H°)/180°$$

where Π is the degree of orientation and *H* represents the width of the half peak height of the I-azimuthal angle curve. The degree of orientation along the orthogonal direction of MXene nanomonomer in the hydrogels was calculated to be ~ 0.75, which indicates that under DC electric field, 2D MXene not only migrated toward the anode, but also orientated orthogonal to the applied electric field.

PNIPAM-based soft hydrogels undergo water expulsion when the temperature is above the lower critical solution temperature (LCST), thus exhibiting a contracting actuation. Due to the higher crosslinking density near the anode side, the dynamics of PNIPAM chains are greatly restricted compared to the opposite side. Herein, upon NIR photothermal heating, water loss in the hydrogel results in a larger contraction of PNIPAM chains near the cathode region, yielding a bending deformation

towards the cathode side (**Figure S15**). The bending angle θ of hydrogel actuators is characterized among hydrogels (MX_aN_1-E_2) with different MXene concentration (a = 5, 10, and 15 mg mL^{-1}) upon identical excitation intensity (808 nm, 0.3 W cm^{-2}). The maximum bending angle was found in sample with moderate MXene concentration (10 mg mL^{-1}) as shown in **Figure 3d, 3e** and **Figure S16-S18**, presumably because excess MXene could pose hurdle for the movement of polymer chains during phase transition. With the same MXene concentration, an increase in electric field strength enables an enhanced shape deformation and faster response speed (**Figure S19**, **S20**). An increase in the thickness of hydrogel actuators $MX_{10}N_1$-E_2 could lead to a decrease of both response speed and bending angle of shape deformation (**Figure S21**). Results of photothermal actuation upon exposure to different light intensities are shown in **Figure 3f**, **Figure S22** and **Movie S1**. It was found that an increased NIR power at 808 nm could prompt both much faster response and larger bending angle of shape deformation, and a large maximum bending angle of 360° could be achieved within 30 s under 0.9 W cm^{-2} of 808 nm NIR irradiation. It should be noted that NIR light-driven actuation process is reversible and reproducible in an aqueous environment for at least 10 actuation cycles without noticeable degradation of performance (**Figure S23**), which might result from the fact that the *in situ* cross-linking of photopolymerizable MXene nanomonomer into hydrogel polymer networks could greatly enhance the stability of MXene-containing anisotropic hydrogel actuators.

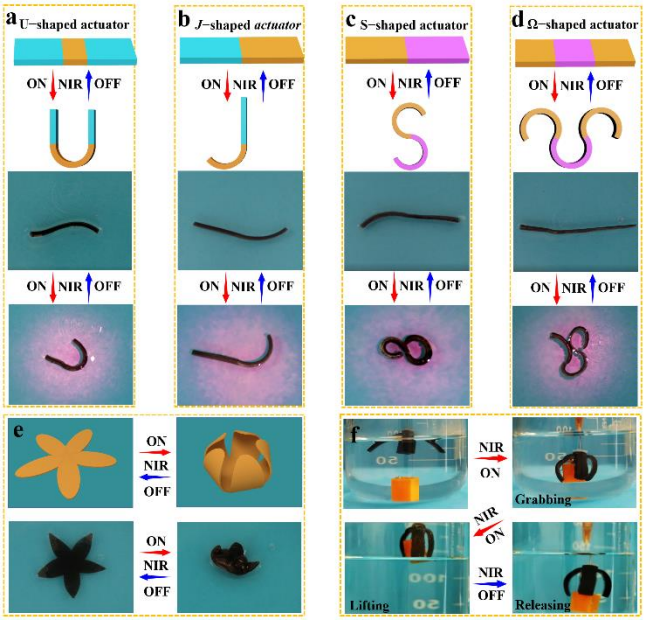

Figure 4. NIR light-driven shape-morphing of programmable MXene-containing anisotropic hydrogel actuators. (a) U-shaped actuator, (b) J-shaped actuator, (c) S-shaped actuator, (d) Ω-shaped actuator. In the schematic illustration, no electric field was applied onto blue part, while positive and negative electric fields were applied onto yellow and pink part, respectively. (e) NIR light-driven reversible open and closing of flower-shaped actuator. (f) NIR light-driven four-arm soft gripper that can perform distinct photomechanical functions including grasping, lifting up, lowering down, and releasing an object. Notes: Actuation was carried out in water at 25 °C under 808 nm NIR irradiation with a power of 0.9 W cm^{-2}.

Taking the advantages of electrically induced anisotropy and on-demand photothermal actuation, light-driven shape-morphing can be achieved in programmable MXene-containing anisotropic hydrogel actuators. Herein, a variety of programmed shapes were demonstrated through ITO electrode patterning, switching the electric field direction and mask-assisted photopolymerization of $MX_{10}N_1$-E_2 hydrogel (**Figure S24**). As shown in **Figure 4a**, when the electric field was only applied onto the middle part of the hydrogel, a reversible U-shape was obtained; When electric field was applied onto one half, a J-shape was made (**Figure 4b**). Furthermore, S-shaped and Ω-shaped hydrogel actuators could be achieved by applying different electrodes and switching the field directions (**Figure 4c, 4d** and **Movie S2**). More complex shape-morphing can also be attained, for instance, an assembly of "hydrogel" letters as shown in **Figure S25**. Taking lessons from nature, we conceptualized a flower-shaped MXene-containing anisotropic hydrogel actuator, which could exhibit reversible opening and closing action in the water upon NIR light irradiation (**Figure 4e** and **Movie S3**). We also demonstrated a NIR light-driven shape-programmed four-arm soft gripper based on MXene-containing anisotropic hydrogels. Upon switching on the NIR light exposure, the soft gripper was able to grasp a cubic cargo, lifting up and taking it out of the water. Then, the gripper was lowered down, putting the object back into the liquid and releasing it after ceasing the light (**Figure 4f** and **Movie S4**). These MXene-containing anisotropic hydrogel actuators with programmable photomechanical functions could provide new insights into the development of untethered, adaptive and reconfigurable soft robotics.

Conclusion

In conclusion, we have reported novel NIR light-driven shape-programmable $Ti_3C_2T_x$ MXene-containing hydrogel actuators, where photopolymerizable MXene nanomonomer was designed and synthesized to promote homogeneous dispersion of exfoliated MXene nanosheets in PNIPAM-based smart hydrogels and *in situ* photopolymerization into 3D crosslinked hydrogel networks. It was found that a gradient distribution of MXene nanosheets across the thickness of the hydrogel actuators could be developed with electrophoresis effects under DC electric field, and the resulting MXene-containing anisotropic hydrogel actuators were found to exhibit fast light-driven directional shape deformation upon 808 nm NIR irradiation thanks to the superior photothermal effect of MXene nanosheets. Taking advantages of electrodriven shape-programming and NIR photothermal actuation of as-prepared anisotropic hydrogel actuators, we demonstrated NIR light-driven shape-morphing of programmable MXene-containing hydrogel actuators with complex deformation, including "U", "J", "S", "Ω" and complex "flower" shapes, through facilely controlling ITO electrode pattern, electric field direction and mask-assisted photopolymerization. We also conceptualized light-driven bioinspired four-arm soft gripper that could perform distinct photomechanical functions including grasping, lifting up, lowering down, and releasing an object upon exposure to NIR light stimulus. The outstanding actuation performances of MXene-containing anisotropic hydrogel actuators could be attributed to the electric field induced inhomogeneous distribution of MXene nanosheets in the hydrogel matrix. The photoresponsive dynamics of the hydrogel actuators were derived from the synergetic combination of different features such as gradient structure across the thickness of the hydrogels, loading concentration of MXene monomer and power density of NIR irradiations. It should be noted that the *in situ* cross-linking of photopolymerizable MXene nanomonomer into hydrogel polymer networks could greatly enhance the stability of MXene-containing hydrogel actuators, thus light-driven actuation process is

reversible and reproducible in an aqueous environment for many cycles without noticeable degradation. The strategy disclosed herein can provide new impetus towards the development of untethered, programmable and reconfigurable smart actuators that can find diverse applications in areas of soft robotics or machines, biomedical devices and beyond.

Acknowledgements

This work was financially supported by National Natural Science Foundation of China (No. 51973155 and 51873147), Postdoctoral Science Foundation of China (No. 2019M661015), and Academy of Finland (Flagship Programme PREIN, No. 320165 and a postdoctoral grant No. 326445).

Keywords: soft robotics • anisotropic hydrogel • MXene • programmable • NIR light

[1] a) Q. Li (Ed.), *Intelligent Stimuli Responsive Materials: From Well-defined Nanostructures to Applications*, John Wiley & Sons, Hoboken, NJ, **2013**; b) K. Sano, Y. Ishida, T. Aida, *Angew. Chem. Int. Ed.* **2018**, *57*, 2532; c) M. P. D. Cunha, M. G. Debije, A. P. H. J. Schenning, *Chem. Soc. Rev.* **2020**, DOI: 10.1039/d0cs00363h; d) H. Zhang, H. Zeng, A. Priimagi, O. Ikkala, *Adv. Mater.* **2020**, 1906619; e) S. J. Jeon, A. W. Hauser, R. C. Hayward, *Acc. Chem. Res.* **2017**, *50*, 161; f) L. Wang, A. M. Urbas, Q. Li, *Adv. Mater.* **2020**, 32, 1801335; g) H. K. Bisoyi, Q. Li, *Chem. Rev.* **2016**, *116*, 15089; h) Q. Li, A. P. H. Schenning, T. J. Bunning, *Adv. Optical Mater.* **2019**, *7*, 1901160.

[2] H. N. Kim, A. Jiao, N. S. Hwang, M. S. Kim, D. H. Kang, D. H. Kim, *Adv. Drug Deliv. Rev.* **2013**, *65*, 536.

[3] a) J. Dumais, Y. L. Forterre, *Annu. Rev. Fluid Mech.* **2012**, *44*, 453; b) R. Elbaum, L. Zaltzman, I. Burgert, P. Fratzl, *Science* **2007**, *316*, 884.

[4] a) H. Zeng, W. Piotr, D. S. Wiersma, A. Priimagi, *Adv. Mater.* **2018**, *30*, 1870174; b) H. Yu, T. Ikeda, *Adv. Mater.* **2011**, *23*, 2149; c) T. J. White, D. J. Broer, *Nat. Mater.* **2015**, *14*, 1087; d) X. Wang, R. Guo, J. Liu, *Adv. Mater. Technol.* **2019**, *4*, 1970009; e) L. Tang, L. Wang, X. Yang, Y. Y. Feng, W. Feng, *Prog. Mater. Sci*. **2021**, *115*, 100702; f) X. S. Qian, Y. Zhao, Y. Alsaid, X. Wang, X. M. He, *Nat. Nanotechnol.* **2019**, *14*, 1048; g) X. X. Le, W. Lu, J. W. Zhang, T. Chen, *Adv. Sci.* **2019**, *6*, 1801584; h) X. L. Pang, J. Lv, C. Y. Zhu, L. Qin, Y. L. Yu, *Adv. Mater.* **2019**, *31*, 1904224; i) F. Lancia, A. Ryabchun, N. Katsonis, *Nat. Rev. Chem*. **2019**, *3*, 536; j) M. Yang, Z. Yuan, J. Liu, Z. Fang, L. Fang, D. Yu, Q. Li, *Adv. Optical Mater.* **2019**, *7*, 1900069; h) Y. Chen, J. Yang, X. Zhang, Y. Feng, H. Zeng, L. Wang, W. Feng, *Mater. Horiz*. **2020**, DOI: 10.1039/D0MH01406K.

[5] a) N. Park, J. Kim, *Adv. Intell. Syst.* **2020**, *2*, 1900135; b) Y. Lee, W. J. Song, J. Y. Sun, *Mater. Today Phys.* **2020**, 100258; c) B. Hritwick, S. Mohamed, H. Ren, *Biomimetics* **2018**, *3*, 15; d) D. J. Beebe, J. S. Moore, J. M. Bauer, Q. Yu, B. H. Jo, *Nature* **2015**, *404*, 588.

[6] a) C. X. Ma, W. Lu, X. X. Yang, X. X. Le, L. Wang, J. W. Zhang, T. Chen, *Adv. Funct. Mater.* **2018**, *28*, 1704568; b) S. X. Wei, W. Lu, X. X. Le, C. X. Ma, H. Lin, B. Y. Wu, J. W. Zhang, P. Theato, T. Chen, *Angew. Chem. Int. Ed.* **2019**, *58*, 16243; c) Y. L. Zhang, Y. Wang, H. Wang, Y. Yu, Q. F. Zhong, Y. J. Zhao, *Small* **2019**, *15*, 1902198; d) Y. Yang, Y. Tan, X. L. Wang, W. L. An, S. M. Xu, W. Liao, Y. Z. Wang, *ACS Appl. Mater. Interfaces* **2018**, *10*, 7688; e) Y. Tan, D. Wang, H. X. Xu, Y. Yang, X. L. Wang, F. Tian, P. P. Xu, W. L. An, X. Zhao, S. M. Xu, *ACS Appl. Mater. Interfaces* **2018**, *10*, 40125.

[7] a) L. Wang, Q. Li, *Chem. Soc. Rev.* **2017**, *47*, 1044; b) C. Li, A. Iscen, H. Sai, K. Sato, N. A. Sather, S. Chin, Z. Àlvarez, L. C. Palmer, G. C. Schatz, S. I. Stupp, *Nat. Mater.* **2020**, *19*, 900; c) Z. G. Zheng, Y. N. Li, H. K. Bisoyi, L. Wang, T. Bunning, Q. Li, *Nature*, **2016**, *531*, 352; d) L. Wang, H. Dong, Y. N. Li, C. M. Xue, L. D. Sun, C. H. Yan, Q. Li, *J. Am. Chem. Soc.* **2014**, *136*, 4480; e) H. Wang, H. K. Bisoyi, L. Wang, A. Urbas, T. Bunning, Q. Li, *Angew. Chem. Int. Ed.* **2018**, *57*, 1627; f) R. Lan, J. Sun, C. Shen, R. Huang, H. Yang, *Adv. Mater.* **2020**, *32*, 1906319.

[8] L. Ionov, *Adv. Funct. Mater.* **2013**, *23*, 4555.

[9] a) A. S. Gladman, E. A. Matsumoto, R. G. Nuzzo, L. Mahadevan, J. A. Lewis, *Nat. Mater.* **2016**, *15*, 413; b) J. E. Stumpel, D. Liu, D. J. Broer, A. P. H. J. Schenning, *Chem. Eur. J.* **2013**, *19*, 10922; c) M. Liu, Y. Ishida, Y. Ebina, T. Sasaki, T. Hikima, M. Takata, T. Aida, *Nature* **2015**, *517*, 68; d) H. Kim, J. Kang, Y. Zhou, A. Kuenstler, Y. Kim, C. Chen, T. Emrick, R. C. Hayward, *Adv. Mater.* **2019**, *31*, 1900932.

[10] a) Y. S. Kim, M. Liu, Y. Ishida, Y. Ebina, M. Osada, T. Sasaki, T. Hikima, M. Takata, T. Aida, *Nat. Mater.* **2015**, *14*, 1002; b) T. Aida, Z. Sun, Y. Yamauchi, F. Araoka, Y. S. Kim, J. Bergueiro, Y. Ishida, Y. Ebina, T. Sasaki, T. Hikima, *Angew. Chem. Int. Ed.* **2018**, *130,* 15998.

[11] a) Q. Zhu, C. Du, Y. Dai, M. Daab, M. Matejdes, J. Breu, W. Hong, Q. Zheng, Z. L. Wu, *Nat. Commun.* **2020**, *11*, 5166; b) Q. L. Zhu, C. F. Dai, D. Wagner, M. Daab, W. Hong, J. Breu, Q. Zheng, Z. L. Wu, *Adv. Mater.* **2020**, DOI:10.1002/adma.202005567.

[12] F. Xiao, S. Naficy, G. Casillas, M. H. Khan, T. Katkus, L. Jiang, H. Liu, H. Li, Z. Huang, *Adv. Mater.* **2015**, *27*, 7196.

[13] W. X. Fan, C. Y. Shan, H. Y. Guo, J. W. Sang, R. Wang, R. R. Zheng, K. Y. Sui, Z. H. Nie, *Sci. Adv.* **2019**, *5*, 7174.

[14] a) Y. Gogotsi, B. Anasori, *ACS Nano* **2019**, *13*, 8491; b) M. Naguib, V. N. Mochalin, M. W. Barsoum, Y. Gogotsi, *Adv. Mater.* **2014**, *26*, 992.

[15] D. Pang, M. Alhabeb, X. P. Mu, Y. Dall'Agnese, Y. Gogotsi, Y. Gao, *Nano Lett.* **2019**, *19*, 7443.

[16] J. F. Wang, Y. Y. Liu, Z. J. Cheng, Z. M. Xie, Z. M. Fan, *Angew. Chem. Int. Ed.* **2020**, *132*, 14133.

[17] G. F. Cai, J. H. Ciou, Y. Z. Liu, Y. Jiang, P. S. Lee, *Sci. Adv.* **2019**, *5*, 11.

[18] Y. Z. Zhang, J. K. El-Demellawi, Q. Jiang, G. Ge, H. Liang, K. Lee, X. Dong, H. N. Alshareef, *Chem. Soc. Rev.* **2020**, DOI: 10.1039/D0CS00022A.

[19] Z. L. Li, H. Zhang, J. Han, Y. Chen, T. Yang, *Adv. Mater.* **2018**, *30*, 1706981.

[20] H. Lin, X. G. Wang, L. Yu, Y. Chen, J. Shi, *Nano Lett.* **2017**, *17*, 384.

[21] a) B. Liu, C. Li, P. Yang, Z. Hou, J. Lin, *Adv. Mater.* **2017**, *29*, 1605434; b) L. Wang, H. Dong, Y. N. Li, R. Liu, Y. F. Wang, H. K. Bisoyi, L. D. Sun, C. H. Yan, Q. Li, *Adv. Mater.* **2015**, *27*, 2065.

Entry for the Table of Contents

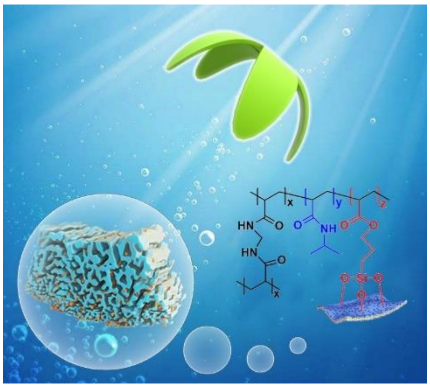

Programmable anisotropic hydrogel actuators with near-infrared (NIR) light-driven shape morphing properties were fabricated through *in situ* free-radical copolymerization of a judiciously designed photopolymerizable MXene nanomonomer with thermosensitive PNIPAM-based smart hydrogels. As a proof-of-concept, a bioinspired shape-programmed four-arm soft gripper was demonstrated to perform distinct photomechanical functions including grasping, lifting up, lowering down, and releasing an object under sequential exposure to spatiotemporal NIR light.